applied sciences

MDPI

Article

Impact of Seat Inclination and Misalignment on Airborne Pollutant Transport in a Single-Aisle Aircraft Cabin

Tengfei (Tim) Zhang [1,2], Mingqi Fan [1] and Sumei Liu [1,*]

[1] Tianjin Key Laboratory of Indoor Air Environmental Quality Control, School of Environmental Science and Engineering, Tianjin University, Tianjin 300072, China; timzhang@tju.edu.cn (T.Z.); fmq21@tju.edu.cn (M.F.)
[2] School of Civil Engineering, Dalian University of Technology, Dalian 116024, China
* Correspondence: smliu@tju.edu.cn

Abstract: Airborne pollutant transport in an aircraft cabin is greatly affected by the created airflow. The seat layout can impact the flow and thus the pollutant transport. Most studies have adopted symmetric upright seats for simplicity. The influence of seat inclination and seat misalignment on airflow and pollutant transport is still unclear. This investigation adopted a validated computational fluid dynamics (CFD) method to study the airflow and airborne pollutant distribution in a single-aisle cabin with seven rows of seats. The pollutant was assumed to be released from a passenger seated in the middle of three adjacent seats. A total of five different seat layouts were considered, including all of the upright seats, the inclination of three adjacent seats, the inclination of all of the seats in half a cabin, the inclination of all of the seats in a whole cabin, and the misalignment seat rows across the aisle. The flows in both the cross and longitudinal sections were compared. The pollutant concentrations in the respiratory zone of the passengers in different seats were adopted to evaluate the cross-contamination. The results revealed that the symmetric seat layout aids to circumscribe the released pollutant in a small region and reduces the cross-contamination either by maintaining the upright seats or inclining all of the seats. Contrarily, any inclination of seats or a misalignment of seat rows should be avoided during the pandemic since an asymmetric seat layout would generate asymmetric flow and strengthen the spreading of pollutants.

Keywords: aircraft cabin; airborne pollutant; airflow; cross-contamination; CFD

Citation: Zhang, T.; Fan, M.; Liu, S. Impact of Seat Inclination and Misalignment on Airborne Pollutant Transport in a Single-Aisle Aircraft Cabin. *Appl. Sci.* **2022**, *12*, 4538. https://doi.org/10.3390/app12094538

Academic Editor: Elza Bontempi

Received: 5 April 2022
Accepted: 27 April 2022
Published: 29 April 2022

1. Introduction

Air travel is related to respiratory infection transport worldwide [1]. On a flight from London to Hanoi, an asymptomatic passenger with COVID-19 was thought to have infected at least 12 passengers [2]. The SARS-CoV-2 is mainly transmitted by short-range aerosol or droplets, long-range aerosol, and surface touch or via the fomite route [3]. Long-range aerosol transport is subjected to the flow in an enclosed space and has been studied extensively recently [4–7]. Due to the stealth transport, the long-range aerosol transport must be paid with sufficient attention in a compact aircraft cabin.

Mixing ventilation is currently used on commercial aircraft [8,9]. Conditioned air is supplied into the cabin at a relatively high speed near the upper sidewalls and the internal air is exhausted out of the cabin near the floor. The seat layout exerts an impact on the cabin geometry and thus may affect the formed cabin airflow therein. Most previous studies adopted a simplified seat geometry [9–16], in which the seat cushion was horizontal and the seatback was upright. Realistic aircraft seats were also used in some studies, which captured more details of the streamlined profiles of the seats [4,17–25]. The adopted manikins varied greatly, ranging from heated rectangular boxes [11,13–16,20,21], to models with realistic body profiles [4,9,10,12,17–19,22]. Table 1 summarizes the seat structure and manikins in the published studies, in which the seat layouts and manikins were symmetric.

Table 1. Summary of symmetric, upright seat layout and manikins in representative published studies.

Airplane Model	Seat Number	Seat Shape	Seat Structure	Manikins	Method	References
B767	49 in 7 rows	Simplified seats	Upright	Realistic body profiles	Measurement	Zhang, 2013 [9]
B767	49 in 7 rows	Simplified seats	Upright	Tealistic body profiles	CFD	Zhang, 2013 [10]
B767	28 in 4 rows	Simplified seats	Upright	Rectangular boxes	CFD	Zhang, 2007 [11]
B767	49 in 7 rows	Simplified seats	Upright	Realistic body profiles	CFD	You, 2019 [12]
B737	42 in 7 rows	Simplified seats	Upright	Realistic body profiles	CFD	You, 2019 [12]
B737	42 in 7 rows	Simplified seats	Upright	Rectangular boxes and cylinders	CFD	Cao, 2022 [13]
B737	42 in 7 rows	Realistic airplane seats	Upright	Realistic body profiles	Measurement	Li, 2015 [17], Li, 2017 [18], Wang, 2017 [19]
B737	36 in 6 rows	Realistic airplane seats	Upright	Rectangular boxes and cylinders	Measurement	Li, 2021 [20]
B737	42 in 7 rows	Realistic airplane seats	Upright	Rectangular boxes and cylinders	Measurement	Liu, 2021 [21]
B737	42 in 7 rows	Realistic airplane seats	Upright	Realistic body profiles	CFD	Yan, 2017 [4]

Even with symmetric geometry in the cabin, there is still a risk of cross-transport. This was because the jet flows from the air-supply inlets in both sides collided in the middle and swung across the aisle [17–19]. The saddle-shaped counter-rotating airflow shifted right-to-left and left-to-right periodically [7], which enhanced cross-transport. It was found that in a single-aisle cabin where the seats and manikins were upright and symmetric, the airflow in the cabin tended to be symmetric, but pollutants could still transmit laterally. A considerable amount of the exhaled contaminants was transported from the release source into the aisle and dispersed to the other half of the cabin [12]. Similarly, in another single-aisle aircraft cabin [20], the measurement showed that the released particles were transported to the other side of the cabin. In a twin-aisle aircraft cabin, the rather symmetric airflow in the cabin was solved by a validated CFD program [11]. The above studies adopted a simplified upright seat layout.

In a realistic cabin, passengers may incline the seats during the flight, which alters the symmetry of the cabin structure, and thus modifies the airflow therein. Some studies have already accounted for the inclined seats [23,25–27] when investigating the cabin airflow and pollutant transport. The seats inclined at 15° in a fully occupied, twin-aisle cabin were claimed to generate a longitudinal flow at around 0.2 to 0.3 m/s [26]. Another study [27] simulated the SARS-CoV-2 transport in a twin-aisle first-class cabin with all passengers lying flat. Table 2 summarizes the representative published studies in which the seats and manikins were inclined with certain angles. So far, the exact impact of seat inclination on airflow patterns and pollutant transport have not been well investigated.

Table 2. Summary of inclined seats in representative published studies.

Airplane Model	Seat Number	Seat Shape	Seat Structure	Manikins	Method	References
Unknown	49 in 7 rows	Simplified Seats	All seats inclined (15°)	Rectangular boxes	CFD	Gupta, 2010 [26]
B787-9	39 in 5 rows	Simplified Seats	All seats lying flat	Cylinders	CFD	Wang, 2021 [27]
B737	60 in 10 rows	Realistic airplane seats	All seats inclined (12.1°)	Cylinders	CFD	Khaled, 2021 [23]
B737	3 in 1 rows	Realistic airplane seats	All seats inclined (unknown angels)	Realistic body	CFD	Yan, 2021 [25]

The asymmetric seat inclination and misalignment may lead to asymmetric airflow and the cross-transport of pollutants. In a half-occupied, twin-aisle cabin mockup, the airflow was found to be asymmetric because of the asymmetric air supply velocity profiles and also the asymmetric manikin occupation mode [14,15]. In a twin-aisle airliner cabin, the seating patterns of passengers were reported to exert a significant impact on the localized airflow and contaminant transport [16]. The airflow in a single-aisle cabin with five passengers in each row (3 passengers + 2 passengers) was found to be asymmetric due to the asymmetric cabin geometry [22]. The asymmetric airflow would enhance the cross-transport of airborne pollutants [15]. Table 3 summarizes the asymmetric seat arrangements in the representative published studies. Different seat occupancy was addressed in these studies, while the seat misalignment had not been focused on so far.

Table 3. Summary of asymmetric seat layouts in representative published studies.

Airplane Model	Seat Number	Reasons for Asymmetric Structure	Seat Shape	Seat Structure	Manikins	Method	References
Unknown	21 in 3 rows	Seat occupancy rate: 15/21	Simplified Seats	Upright	Rectangular boxes	CFD	Wan, 2009 [14]
Unknown	28 in 4 rows	Seat occupancy rate: 14/28	Simplified Seats	Upright	Rectangular boxes	CFD	Zhang, 2009 [15]
Unknown	18 in 4 rows	Seats staggered	Simplified Seats	Upright	Rectangular boxes	CFD	Sagnik, 2008 [16]
MD-82	25 in 5 rows	3 + 2 passengers in each row	Realistic airplane seats	Upright	Realistic body profiles	Measurement	Li, 2016 [22]

The above review revealed that an asymmetric configuration of the aircraft cabin will lead to asymmetric airflow patterns and thus enhance the cross-transport of airborne pollutants. However, the exact impacts of seat inclination and seat misalignment on airflow and airborne pollutant transport is still unclear. The objective of this investigation was to evaluate how the seat inclination and misalignment would affect airflow and airborne pollutant transport. A CFD program was used to explore the airflow and airborne pollutant transport in a single-aisle aircraft cabin mockup. Both the seat inclination and seat misalignment were considered.

2. Method

This section addresses the designed cases with different seat layouts in a single-aisle aircraft cabin and numerical solution strategies.

2.1. Case Design and Boundary Conditions

A fully occupied, single-aisle aircraft cabin containing seven rows of seats was chosen for study. The dimension of the cabin was 5.852 m (Z) × 3.253 m (X) × 2.155 m (Y). A total of 42 thermal manikins were seated inside the cabin. The size of the manikin was close to

an adult, with a sitting height of 1.26 m and a total surface skin area of 1.91 m^2. All of the seats and manikins were upright and symmetric in the reference case, as shown in Figure 1. Conditioned air was supplied into the cabin from the slot opening below the ceiling on both sides. The cabin air was extracted from the slot outlets near the floor. The width of the side air-supply opening was 15 mm. The air-supply direction was slightly downward at a 30°angle from the horizontal direction. The width of the bottom air-exhaust opening was 65 mm. ASHRAE Handbook [28] recommends a minimum flow rate of 9.4 L/s per passenger. Therefore, the total air supplied into the cabin was 1436 m^3/h, corresponding to an average ventilation rate of 9.5 L/s per person. The cabin geometric model and the adopted design parameters were identical to those used in our previous measurement study [20].

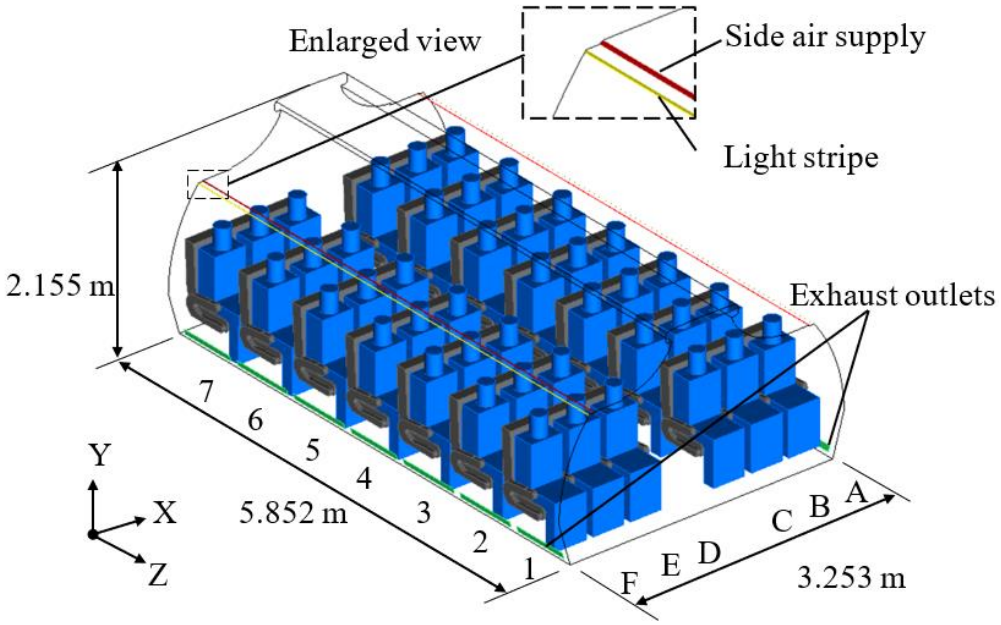

Figure 1. Geometric model of the aircraft cabin in the reference case (Case 1).

To investigate the impact of the seat layout on the cabin flow and the airborne pollutant transport, both the seat inclination and the seat misalignment were studied. The seat inclination was divided into three scenarios. Figure 2a addresses the scenario with three adjacent seats 4A to 4C inclined. Figure 2b presents the scenario with all of the seats A to C in half a cabin inclined, while in Figure 2c all of the seats in the whole cabin were inclined. When inclining the seats, the seats were pressed backward with the seatback inclined 30° from the vertical position. The misalignment of the seats across the aisle is illustrated in Figure 2d without inclining the seats. This was to examine the impact of only the seat misalignment on the flow and pollutant transport. Table 4 summarizes the case design in this investigation. Case 1 was set as the standard reference case, with all of the seats in an upright and symmetric layout. Cases 2 to 4 addressed the seat inclination, while the seat misalignment was considered in Case 5. When inclining the seats, the manikins were also inclined with their backs against the seatbacks.

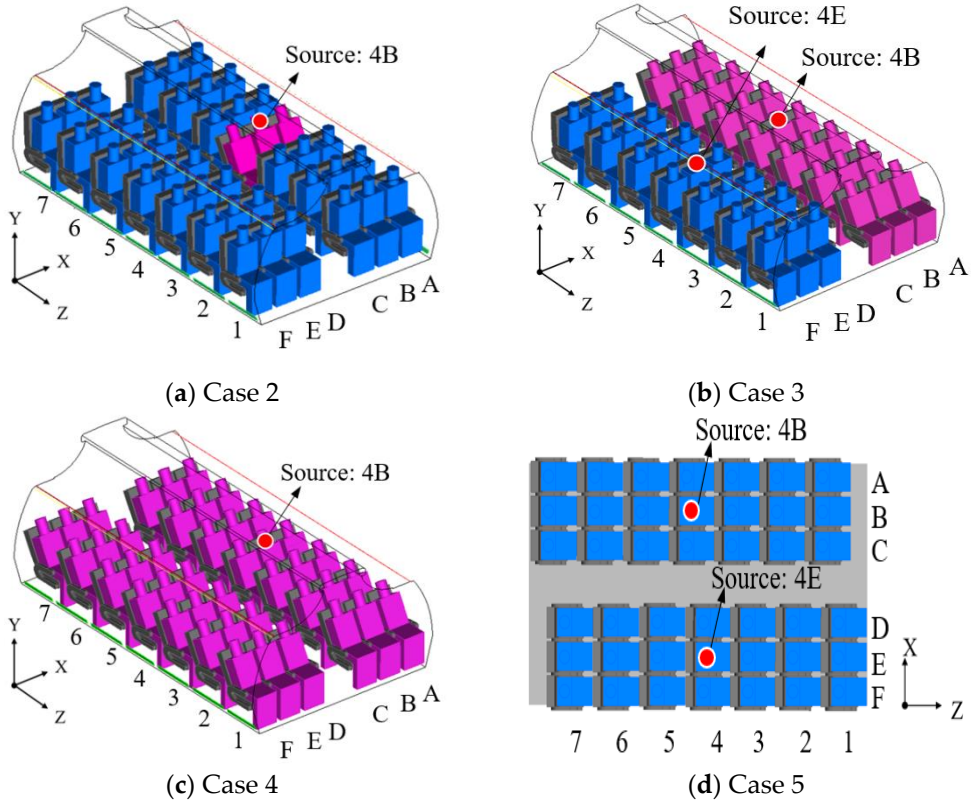

(**a**) Case 2 (**b**) Case 3

(**c**) Case 4 (**d**) Case 5

Figure 2. Geometric models of the aircraft cabin with different seat arrangements: (**a**) seats 4A to 4C inclined, (**b**) seats A to C inclined, (**c**) all of the seats inclined, (**d**) planar view of misaligned seat rows.

Table 4. Case design overview.

Case	Seat Layout	Illustration	Assumed Pollutant Source Position
1	Upright seats in symmetric layout	Figure 1	4B, 4E
2	Only seats 4A to 4C inclined	Figure 2a	4B
3	Seats inclined in half a cabin	Figure 2b	4B, 4E
4	All seats inclined but in symmetric layout	Figure 2c	4B
5	Misaligned seat rows	Figure 2d	4B, 4E

As shown in Table 4, the airborne pollutant was assumed to release from the exhalation of the passengers seated in 4B and 4E in Case 1, Case 3, and Case 5. In Case 2 and Case 4, the pollutant was assumed only in 4B, considering the geometry in the cabin was almost symmetric. When releasing pollutants, the realistic breathing cycle through only the nose was considered. To reduce the computing load, only the manikins seated in the fourth row were assigned respiration. According to [29], two nostril openings each with an area of 0.65 cm^2 were set up, as shown in Figure 3. The breathing profile was close to a sinusoidal wave with a cycle period of 4.4 s and a peak inhalation and exhalation rate of 0.37 L/s as:

$$Q = 0.37 \sin(1.43\,t) \quad (1)$$

where Q is the transient respiration rate, L/s. The θ_m and Φ_m of the exhalation jets were 60° and 69°, respectively, as shown in Figure 3, according to the recommendation in [29]. The exhaled air temperature was assumed to be 33 °C. The above breathing profile was adopted as the boundary condition at the nostril openings.

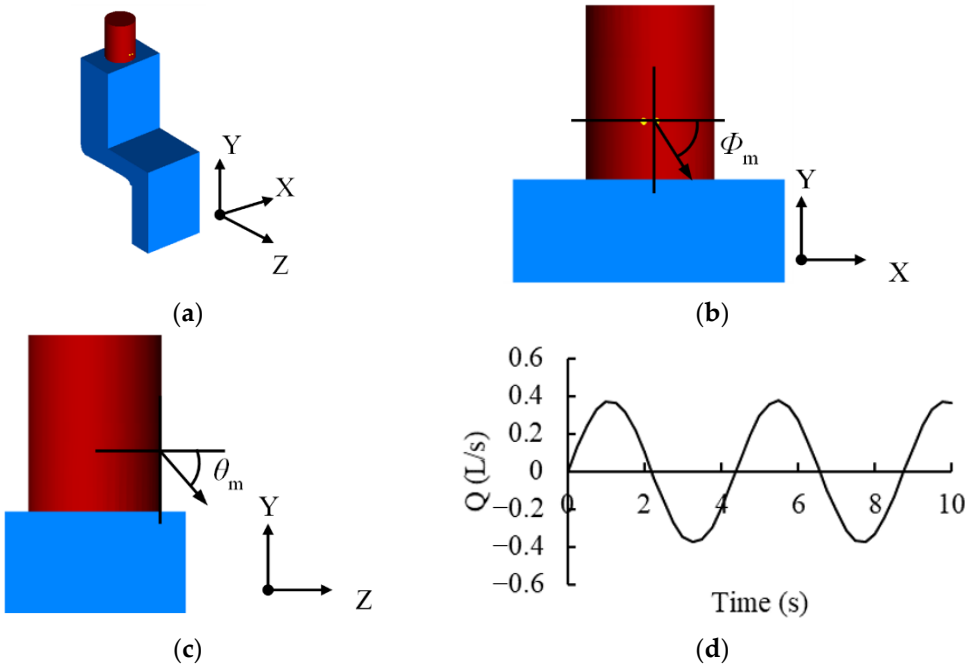

Figure 3. Model for breathing simulation: (**a**) geometric model of the manikin, (**b**) front view of the manikin head, (**c**) side view of the manikin head, (**d**) breathing cycle.

Table 5 lists the major thermo-flow boundary conditions. The aircraft cabin at the cruising stage was considered. The cabin air pressure was set to 85 kPa, which was lower than that at sea level. The cabin surfaces were assigned with a fixed temperature, while the seat was treated as adiabatic. The manikin skin surface temperature was assigned to 30.1 °C [26,30] to reproduce the metabolic heat release.

Table 5. Major thermo-flow boundary conditions.

Parameter	Value	Parameter	Value
Cabin air pressure	85 kPa	Ceiling temperature	22 °C
Ventilation rate per person	9.5 L/s	Lighting temperature	29.4 °C
Width of air-supply opening	15 mm	Side wall temperature	22 °C
Air-supply speed	2.43 m/s	Floor temperature	23 °C
Air supply direction from the horizontal	30°	Manikin skin temperature	30.1 °C
Air-supply temperature	19.4 °C	Exhalation air temperature	33 °C
Width of air-exhaust opening	65 mm	Seat	Adiabatic

2.2. Numerical Model and Solution Strategies

To solve the governing equations of fluid flow, heat, and species transport, this investigation used a commercial CFD software program (ANSYS Fluent 19.0). The RANS CFD solved a series of differential equations that can be cast into the general scalar format as:

$$\frac{\partial}{\partial t}(\rho\phi) + \frac{\partial}{\partial x_j}(\rho u_j \phi) = \frac{\partial}{\partial x_j}\left(\Gamma_{\phi,eff}\frac{\partial \phi}{\partial x_j}\right) + S_\phi \quad (2)$$

where ρ is the air density, φ stands for the velocity component, internal energy, and species concentration in the momentum, energy, and species equations, respectively, t is time, u_j is the velocity component in three directions (x_j, j = 1, 2, 3) of a Cartesian coordinate system, $\Gamma_{\varphi,eff}$ is the effective diffusion coefficient, S_φ is the source term. This study adopted the species model to model the airborne pollutant transport, considering that the exhaled

particles commonly ranged from 0.3 μm to 0.5 μm [31]. Such ultrafine particles could be simplified as a species of gas. The species fraction was set to 1 at the nostril openings.

Most previous investigations [10,12] used the RNG k-ε model to model the turbulent flows in the aircraft cabin. Li et al. [32] also recommended the RNG k-ε model for its comparable performance with the RSM model but less computationally demanding in aircraft cabins. Therefore, this investigation adopted the unsteady RNG k-ε model for turbulence simulation. The numerical method uses the SIMPLE algorithm to couple the pressure and velocity equations. The discretization scheme for pressure is PRESTO! The second-order upwind schemes were adopted to discretize the convection and viscous terms of the governing equations. The steady-state airflow pattern in the cabin was resolved first and set as the initial condition for the transient solution. According to Wang et al. [21], the time step should be less than the jet collision cycle. Therefore, this investigation adopted a time step of 0.1 s in the transient simulation. The results were judged to have reached convergence when the relative residuals of all of the independent variables were less than 10^{-3}.

ANSYS ICEM was used to create the geometry and generate grid meshes. Because of the complexity of the geometric model, this study used the tetrahedral grid scheme. We tested three different grid sizes with a total grid cell number of 6.05 million, 10.09 million, and 18 million. The grid independence analysis results can be found in Figure A1. The grid cell number of 10.09 million was found to provide grid-independent results. The grid cell sizes at the air-supply inlets, manikin surfaces and seats, and the internal space were 10 mm, 25 mm, and 50 mm, respectively. A grid size function with a growth rate of 1.2 was adopted to increase the grid size gradually.

The normalized pollutant concentration C^* was employed to evaluate the cabin air quality as:

$$C^* = \frac{C_{local} - C_{in}}{C_{out} - C_{in}} \quad (3)$$

where C_{local}, C_{in}, C_{out} were the concentration in the respiratory zone, the concentration in the air supply, and the average concentration in the exhaust outlet, i.e., the average concentration in the final returning air duct, respectively. The value of C_{in} was zero in this investigation. The respiratory zone was defined as a cubic with a size of 0.305 m around the nose of each passenger.

2.3. Numerical Model Validation

To validate the CFD model, the measurement data obtained from an aircraft cabin mockup [20] were used. Figure 4 shows the geometry of the cabin mock-up, which was similar to that used in Case 1 as the reference case. However, only the front six rows of seats were seated with the thermal manikins. The total air-supply rate into the cabin was 9.5 L/s per passenger, of which 60% was from the side air supply and 40% from the middle ceiling air supply. The air distribution in the cross-section across the fourth row and the steady-state concentration fields in the cross-section across the fourth row and the longitudinal section across the Cth column were measured. The polydisperse Di-ethyl-hexyl-sebacate (DEHS) particles were released on the head of manikin 4B by a perforated plastic ball at a fixed rate. The test instruments used to measure airflow were three ultrasonic anemometers mounted on a guide rail. The resolution of air velocity was 0.005 m/s with an accuracy of 1%. The particle concentration was measured with an aerodynamic particle size spectrometer (type: 3321; TSI, USA). The resolution of particle counting was 0.001 particles/cm^3, with an accuracy of ±10% plus the statistical deviation. Only the particles at 1 μm were analyzed. More details on the boundary conditions and the measurement can be found in [20].

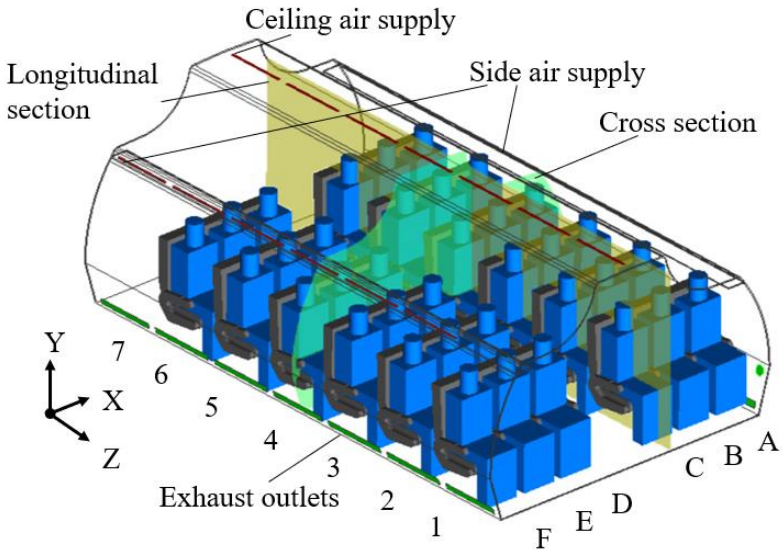

Figure 4. The geometry of the cabin mock-up.

Again, the RNG *k*-ε model together with the standard wall function was adopted for turbulence modeling. The steady-state flow field was solved first and then the transient solution to both flow and particle concentration was switched on. Both the flow and temporal particle concentrations for a total of 700 s were solved.

3. Results

3.1. Model Validation Results

Figure 5a compares the simulated and measured steady-state airflow distribution in the section across the fourth row. The experimental test data can also be found in one of our previous publications [20]. The downward jet flow in the aisle was relatively strong, which separated the two large vortexes on both sides of the cabin. The major flow pattern and the velocity magnitudes were in good agreement between the CFD and the measurement. However, there were some deviations in the downward jet directions in the aisle. This was ascribed to the unstable swinging flow in the aisle, which was beyond the capability of the steady-state modeling.

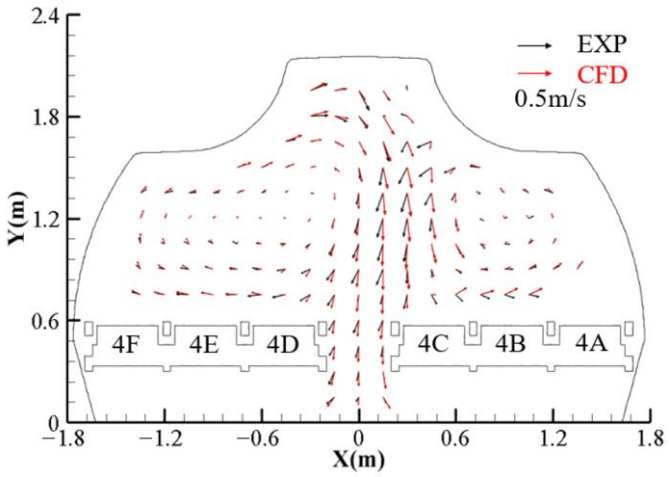

(**a**)

Figure 5. *Cont.*

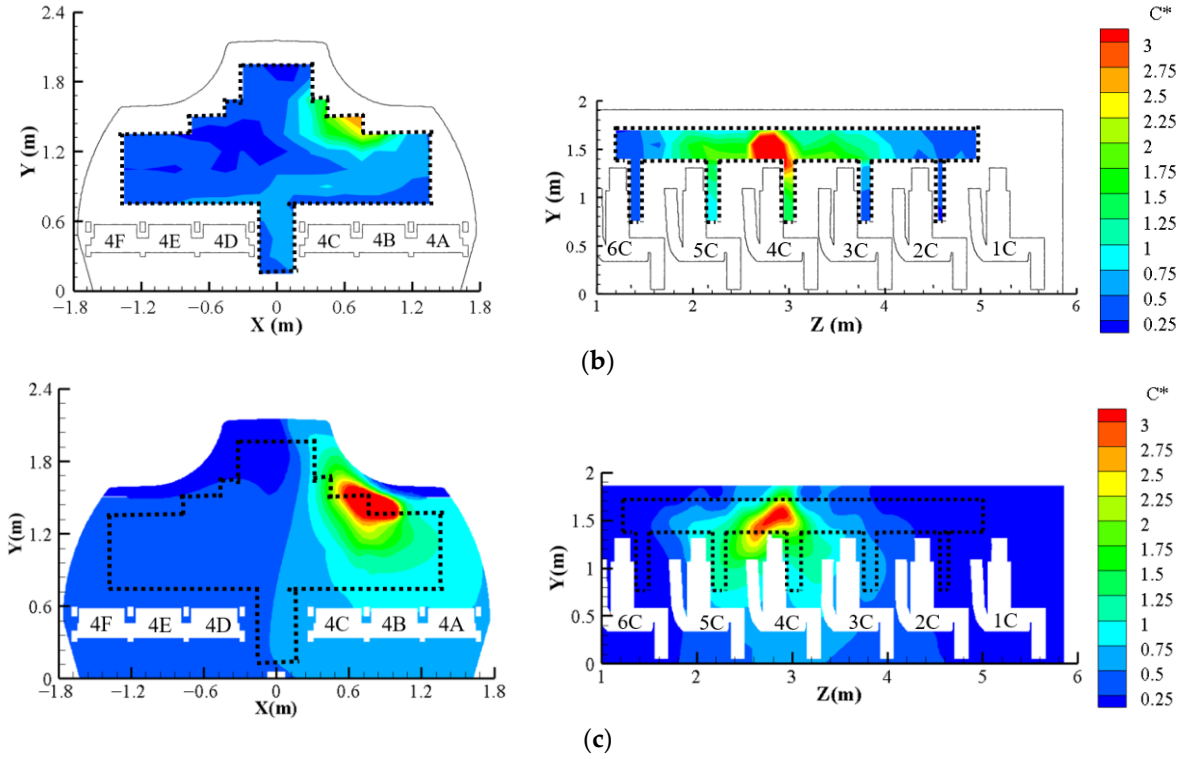

Figure 5. Validation of CFD model: (**a**) comparison of airflow field in a cross-section across the fourth row, (**b**) the steady-state concentration fields of dimensionless particle concentrations by measurement, (**c**) the steady-state concentration fields of dimensionless particle concentrations by CFD simulation.

Figure 5b,c compare the CFD modeled and measured steady-state dimensionless concentration fields of particles in the cross-section across the fourth row and the longitudinal section across the C^{th} column. The simulated particle concentration fields were generally similar to the measurement results. In the cross-section, the high particle concentration was concentrated in the region near the ceiling above seats 4B and 4C, and the particle was transmitted to the left half cabin, which was captured well by CFD. In the longitudinal section, the particles were spread further forward in the measurement than in the CFD, which may be caused by both the longitudinal airflow and the turbulence. It should also be noted that during measurements, the movement of the three-dimensional guide rails mounting the measuring instruments could induce certain disturbances to the flow field and promote particle dispersion.

To further evaluate the CFD results, the normalized root-mean-square error (RMSE) was used to describe the discrepancy with the measurement data [13,32] as:

$$RMSE(C_{pi}, C_{mi}) = \sqrt{\frac{\sum_{i=1}^{n}(C_{pi} - C_{mi})^2}{\sum_{i=1}^{n} C_{mi}{}^2}} \quad (4)$$

where C_{pi} and C_{mi} represent the predicted results and measured data, respectively, such as air velocity and particle concentration at certain locations. Dimensionless velocity and concentration were defined as:

$$V^* = \frac{V_{local}}{\overline{V}}, C^* = \frac{C_{local} - C_{in}}{C_{out} - C_{in}}, \text{ and} C_{in} = 0 \quad (5)$$

where $\overline{V}$ is the average velocity at all of the measured locations, and V_{local} and C_{local} are the air velocity and particle concentration, respectively, at a given location [13,32].

The factor of two observations (FAC2) [33] is another metric used to evaluate the discrepancy between the measurement and the modeling as:

$$FAC2 = \frac{1}{n}\sum_{i=1}^{n} N_i \text{ with } N_i = \begin{Bmatrix} 1 & for\ 0.5 \le \frac{C_{pi}}{C_{mi}} \le 2.0 \\ 1 & for\ C_{mi} \le W\ and\ C_{pi} \le W \\ 0 & else \end{Bmatrix} \quad (6)$$

where W is the absolute difference. W was 0.003 [33] for the normalized contaminant concentration.

As shown in Table 6, the RMSEs in this study were smaller than those reported in [13]. The FAC2 for particle concentrations was 0.67, which was greater than 0.5. In summary, the CFD simulation provided the airflow field and particle concentrations in generally good agreement with the experimental measurements.

Table 6. The RMSE discrepancy between the measurement and the CFD modeling for the velocity and particle concentration.

	Velocity	Concentration
Validation in this study	0.396	0.481
Validation in the literature [13]	0.455	0.551

3.2. Flow and Pollutant Transport in the Reference Case (Case 1)

Figure 6a shows the modeled airflow distribution in the cross-section across the thighs of the manikins in the fourth row when adopting the symmetric, upright seat layout. The airflow from the air-supply inlets in both sides of the aircraft cabin swept the ceiling and then travelled down in the aisle. Two large vortices in the cabin were formed with relatively low speeds in the respiratory zone of the passengers seated in the middle and aisle seats. Part of the airflow in the aisle went outward above the thighs and flowed upward. The other flow swept the floor and went to the air exhaust. With a symmetric geometry setting in the reference case, the computed airflow was nearly symmetric. The flow in the cross-section was relatively strong, which would aid in exhausting the pollutants but also result in cross-contamination. Figure 6b shows the airflow distribution in the longitudinal section across the center of seat 4B. The airflow mainly flowed upward due to the flow recirculation, blocked by the upright seats, and the thermal buoyancy, as shown in Figure 6b. The velocity magnitude near the passengers in the longitudinal section was generally smaller than 0.3 m/s.

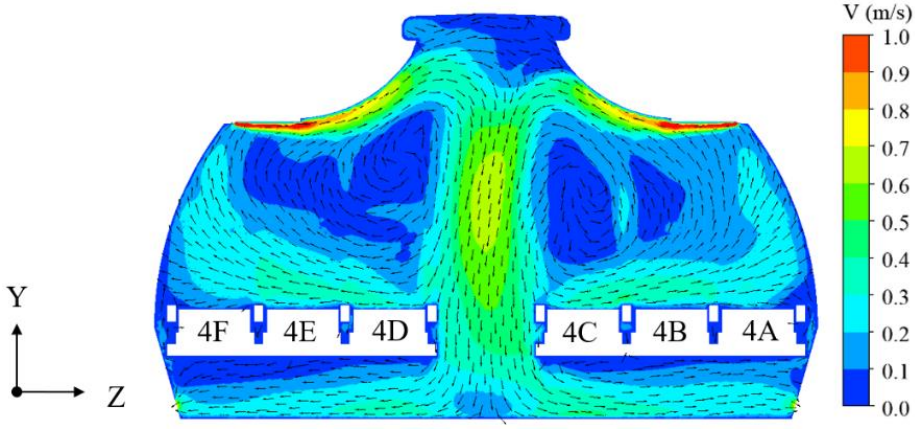

(**a**)

Figure 6. *Cont.*

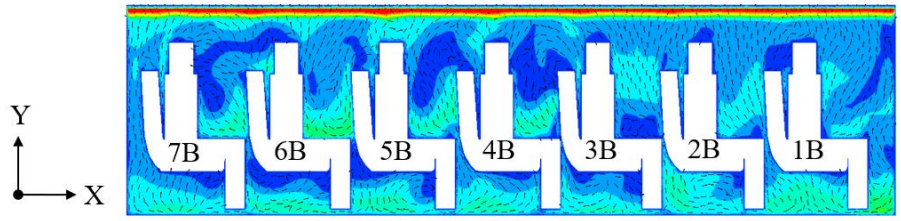

(**b**)

Figure 6. The modeled airflow distributions in Case 1: (**a**) airflow field in the cross-section across the fourth row, (**b**) airflow field in the longitudinal section across the B^{th} column.

To assess the pollutant spread and possible exposure, the discrete pollutant source was hypothetically set to passenger 4B and 4E, respectively. Figure 7a shows the modeled steady-state, averaged normalized pollutant concentrations in respiratory zones of different passengers for the source at 4B, and Figure 7b is for the pollutant source at 4E. The red arrow in the figure designates the pollutant source location. The pollutant spreading region was concentrated in two rows in front of and two rows behind the source, as shown in Figure 7c,d. The pollutant concentrations near the source were generally higher. The concentration in the half cabin where the pollutant source was located was also higher than that in the other half cabin without the pollutant source. This was due to the formed air curtain in the aisle as shown in Figure 6a. With a symmetric seat arrangement, the pollutant spread between sources of 4B and 4E was quite similar. The above results were used as the reference benchmark when changing the seat arrangements in the following investigation.

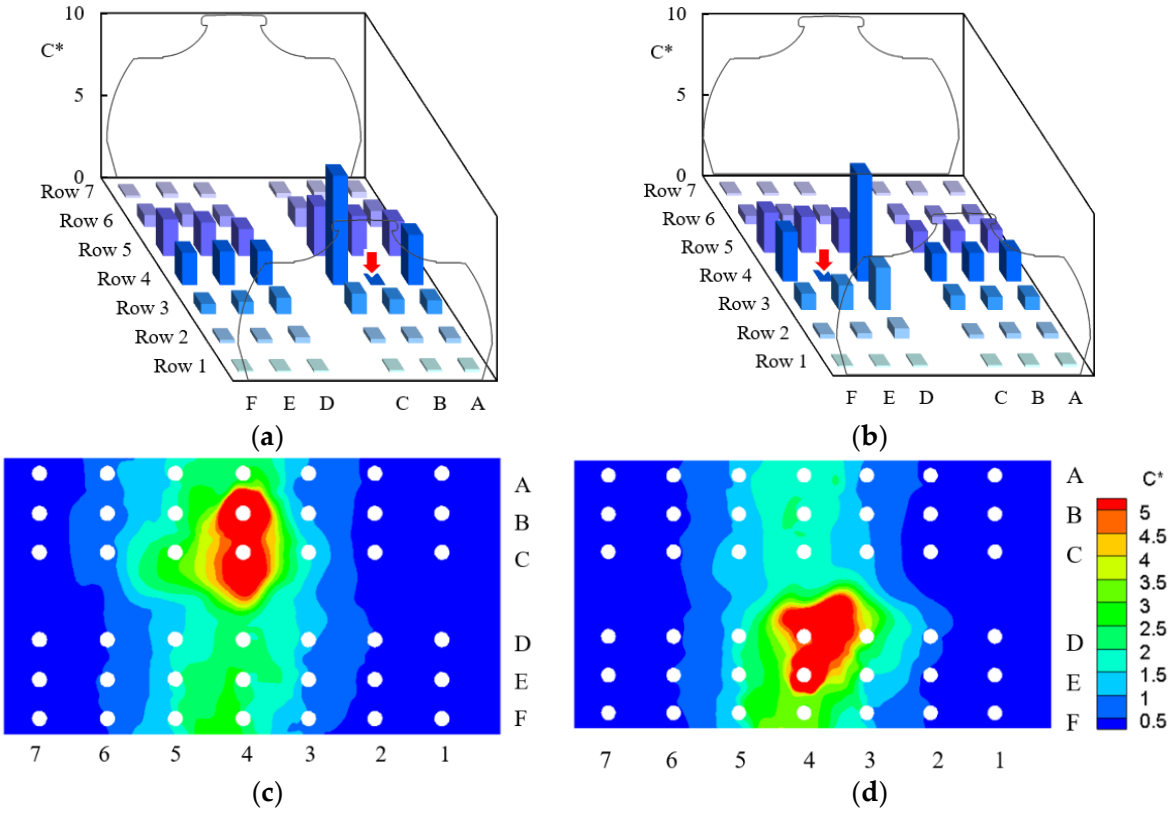

Figure 7. Normalized pollutant concentrations: (**a**) in respiratory zones of passengers in different seats for pollutant source at seat 4B, (**b**) in respiratory zones of passengers in different seats for pollutant source at seat 4E, (**c**) concentration distribution on a horizontal plane of the passenger's nostril height for pollutant source at seat 4B, (**d**) concentration distribution on a horizontal plane of the passenger's nostril height for pollutant source at seat 4E.

3.3. Influence of Cabin Seat Inclination on the Transport of Pollutants

This section examines the impact of seat inclination on the change in the cabin airflow and the transport of pollutants. Figure 8a shows the modeled airflow distribution in a section across the seats of the fourth row, in which seats 4A to 4C were inclined, i.e., in Case 2. As can be seen by comparing Figure 8a with Figure 5a, the inclination of seats 4A to 4C had only a small impact on airflow. However, the uprising flow in front of seats 4A to 4C was weakened somehow, because the trunks of passengers were moved back with the inclined seats and thus there was a larger separating distance between the human bodies and the section. The uprising plume flow decreased with the separating distance from the human bodies. Consequently, the pollutant released at 4B would be better confined in the half cabin with seats A to C. Figure 8b presents the average pollutant concentrations in respiratory zones of the 21 passengers in seats D to E and the comparison between Cases 1 and 2. It is thus not surprising that the concentration in Case 2 was slightly lower than that in Case 1.

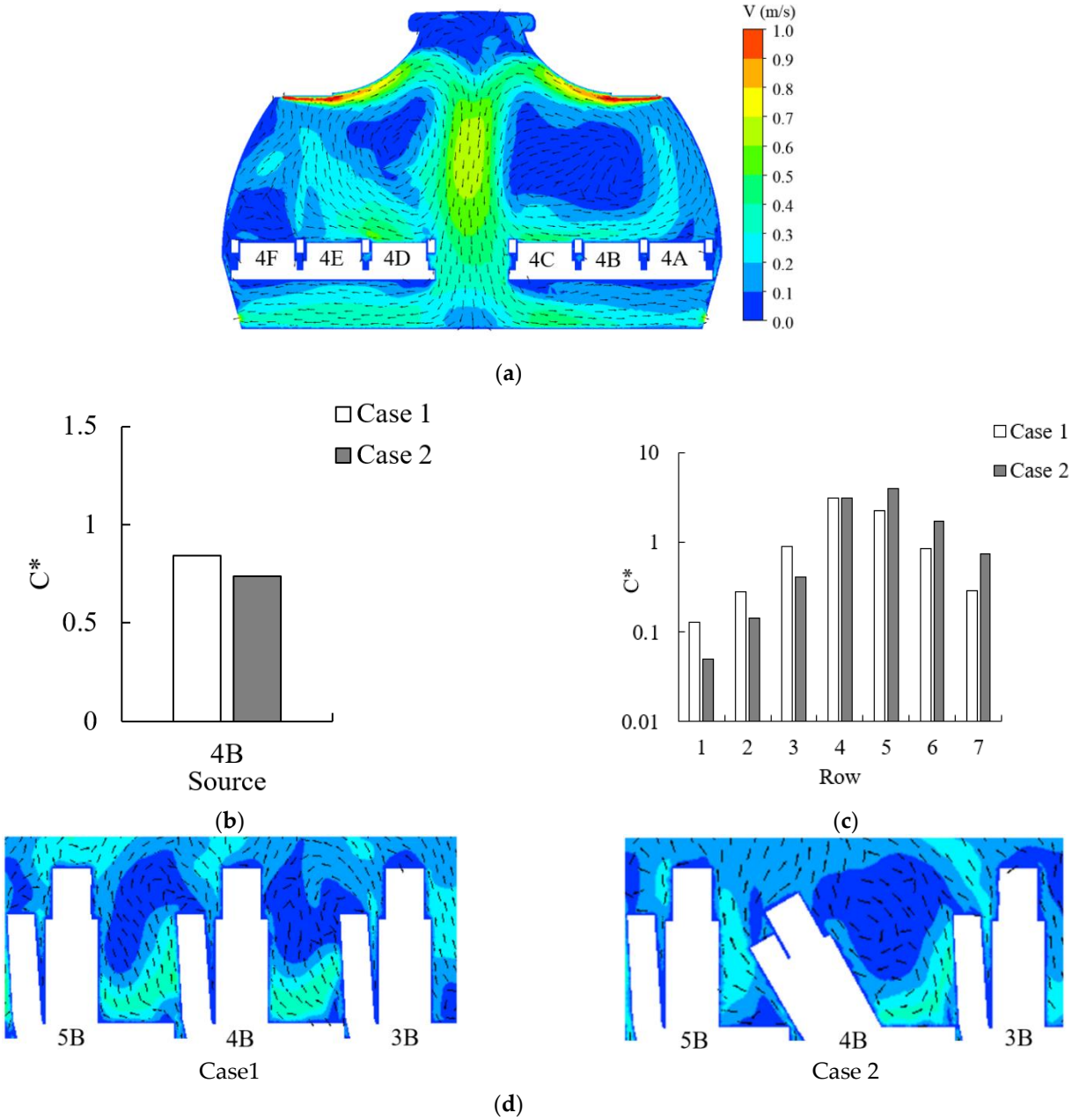

Figure 8. Airflow and normalized pollutant concentrations with seats 4A to 4C inclined in Case 2:

(**a**) airflow field in a section across the fourth row, (**b**) average pollutant concentration in respiratory zone of the 21 passengers seated in D to E for the pollutant released from 4B, (**c**) average pollutant concentrations in respiratory zone of the passengers in each row for the pollutant released from 4B, (**d**) airflow in the longitudinal section from 3B to 5B.

Figure 8c presents the modeled average pollutant concentrations in passengers' respiratory zones of each row between Cases 1 and 2. The seat inclination resulted in an increase of 87% in pollutant concentration in rows 5 to 7, but a decrease of 54% in concentration in rows 1 to 3. This was because there was a smaller separating distance between seats 4A to 4C and seats 5A to 5C. The effect of the seat inclination was somewhat similar to that of positioning the pollutant source to a closer distance with rows 5 to 7, while a longer distance was presented with rows 1 to 3. Figure 9a,b present the modeled flows in two cross-sections when all of the seats A to C were inclined, i.e., in Case 3. The figure shows that some of the flow from the left half cabin crossed the aisle, and went to the right side. This shows that the asymmetric seat layout had clearly led to the asymmetric flow pattern. Consequently, the cross-pollutant transport across the aisle would be enhanced. Figure 9c presents the modeled average pollutant concentration in the respiratory zone of the half cabin opposite to the pollutant source. For the pollutant released from 4B, there was nearly no difference in the pollutant concentrations in the respiratory zone of the 21 seats of D to E. This was because the airflow from the left air supply had suppressed the airflow from the right air supply in the section across the head of 4B, as shown in Figure 9a. This made the pollutant from the right side of the cabin difficult to transmit to the left side of the cabin. However, for the pollutants released from 4E, the seat inclination in Case 3 has resulted in the concentration in the respiratory zone of the 21 seats of A to C increasing by approximately 81%. The major reason was that the flow above seats of 4D to 4E went across the aisle as shown in Figure 9b.

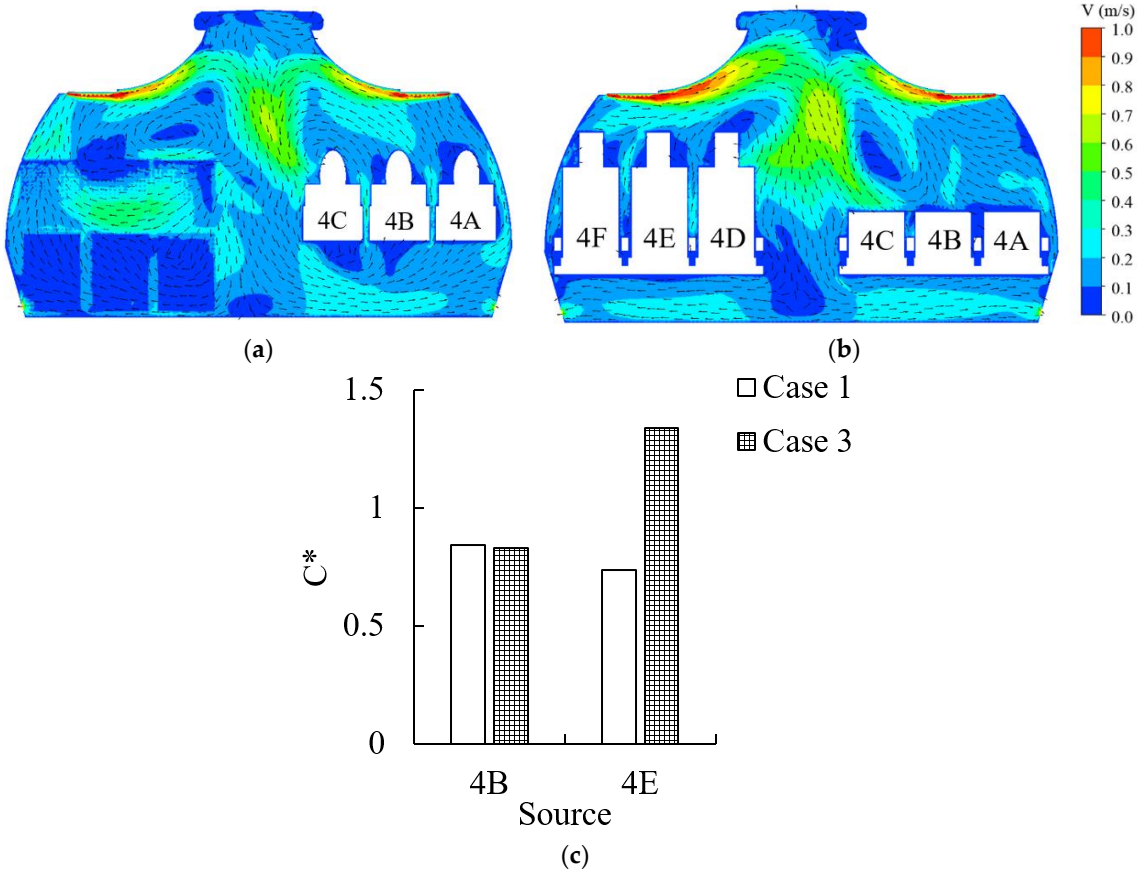

Figure 9. Airflow and normalized pollutant concentrations with all of the seats A to C inclined in

Case 3: (**a**) airflow field in the cross-section across the head of 4B, (**b**) airflow field in the cross-section across the head of 4E, (**c**) average pollutant concentration in respiratory zone of the 21 passengers seated in opposite to the half cabin with pollutant source.

Figure 10a shows the modeled airflow distribution in a section across the fourth row with all of the inclined seats, i.e., in Case 4. Since the seat layout was symmetric, the solved airflow was also nearly symmetric. By comparing this with the airflow in Case 1, the airflow in Case 4 was slightly weaker due to a slightly farther distance of the section with the human body. With a symmetric flow pattern, the modeled average pollutant concentration in the respiratory zone of the 21 passengers in seats D to F was nearly identical between Cases 1 and 4, as shown in Figure 10b. This implies that the inclination of all of the seats did not alter the macroscopic flow in the cabin and the pollutant transport across the aisle very much.

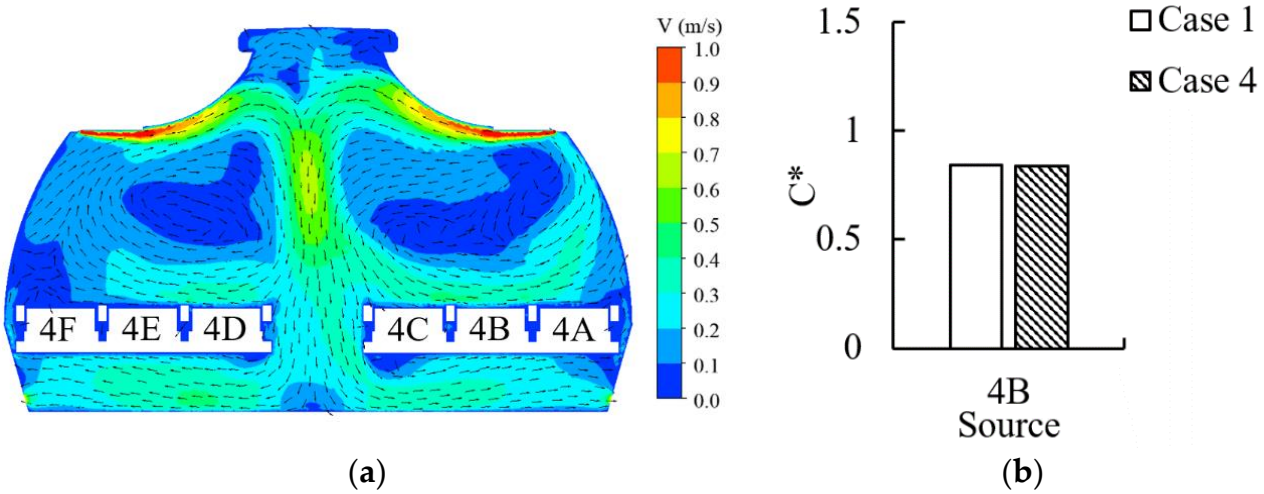

Figure 10. Airflow and normalized pollutant concentrations with all of the seats inclined in Case 4: (**a**) airflow field in the cross-section across the fourth row, (**b**) average pollutant concentration in respiratory zone of the 21 passengers seated in opposite to the half cabin with pollutant source.

To evaluate the impact of seat inclination on the longitudinal transport of pollutants in Cases 3 and 4, the modeled average concentrations in the respiratory zone of the passengers in each row and the comparison with Case 1 are presented in Figure 11a. The pollutant source was at 4B. With inclined seats in Case 4, the pollutant concentrations were higher than those in Case 1 in rows of 1 to 3 but lower than those in Case in rows of 5 to 7. However, there was not much difference in the concentrations between Cases 1 and 3. Among the three cases, the concentration in row 4 was the highest and the concentration decreased gradually with an increase or decrease in the seat rows. Figure 11b shows the modeled airflow distribution in the longitudinal section. When the seats were inclined, the longitudinal airflow was generated only near the passengers. The above results indicate that the seat inclination did not impact much the longitudinal airflow pattern and the basic pollutant distribution in the longitudinal section.

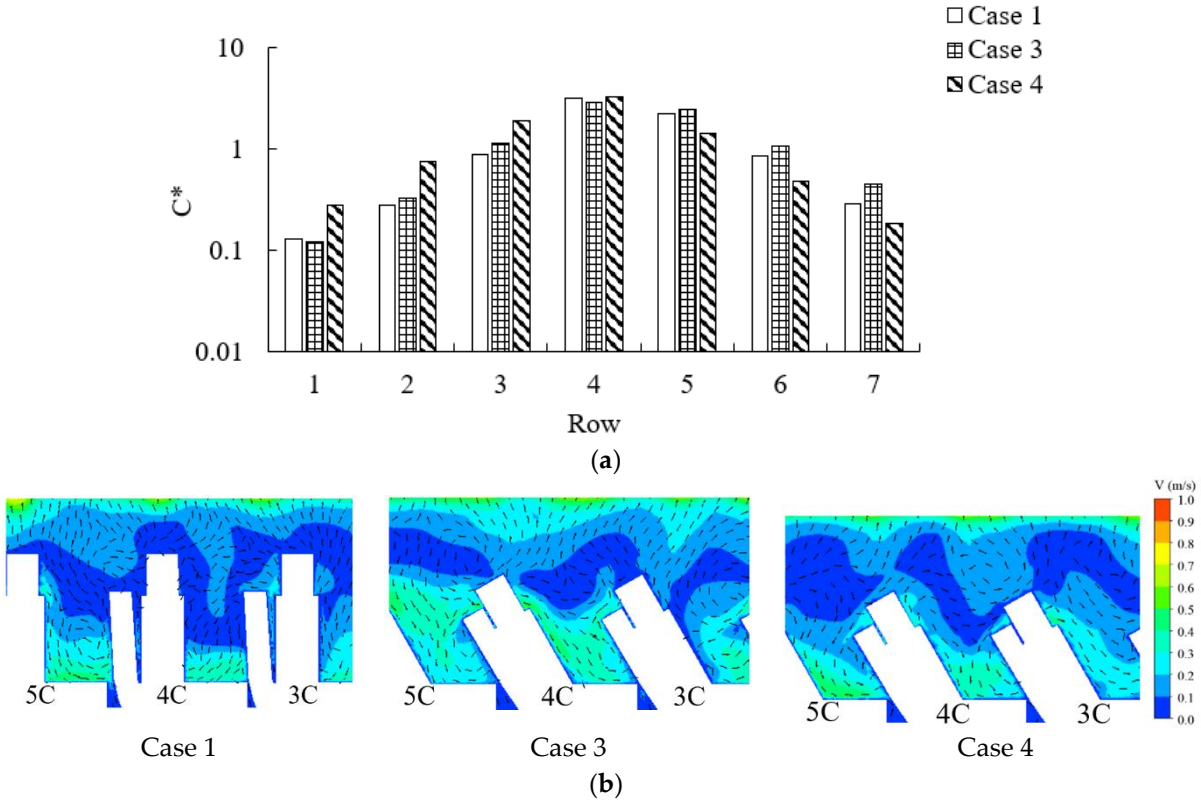

Figure 11. Comparison of normalized pollutant concentration and airflow in Cases 1, 3, and 4: (**a**) average pollutant concentrations in the respiratory zone of the passengers in each row for the pollutant released from 4B, (**b**) airflow distribution in the longitudinal section from 3C to 5C.

3.4. Impact of Misalignment of Seat Rows on the Transport of Pollutants

Figure 12a presents the modeled airflow in the section across the heads of the passengers sitting in seats 4A to 4C. The supplied airflow in the right half cabin with seats 4A to 4C went to the left half cabin and the flow swept the legs of passengers sitting in seats 5D to 5F. Similarly, as shown in Figure 12b the supplied airflow in the left cabin with seats 4D to 4F went to the right half cabin and swept the thighs of the passengers seated in 4A to 4C. The above clearly indicated that the seat misalignment promoted the flow across the aisle, which might enhance the cross-contamination in the cross-section.

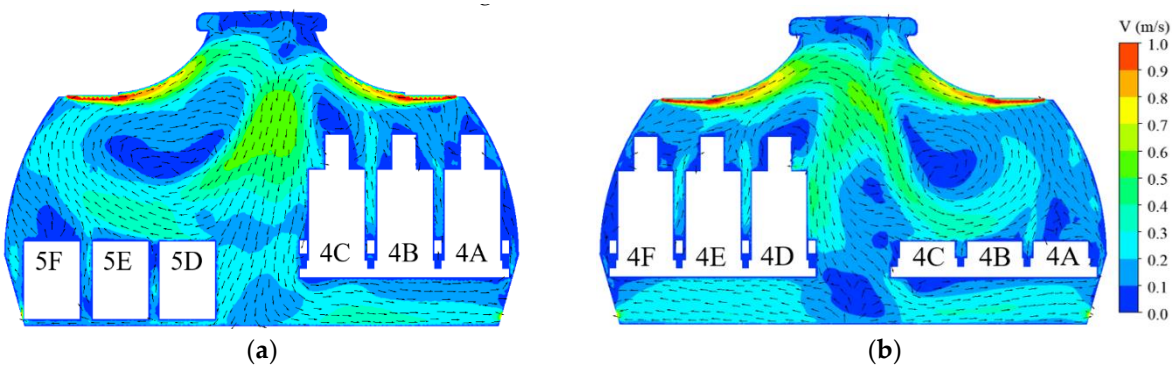

Figure 12. *Cont.*

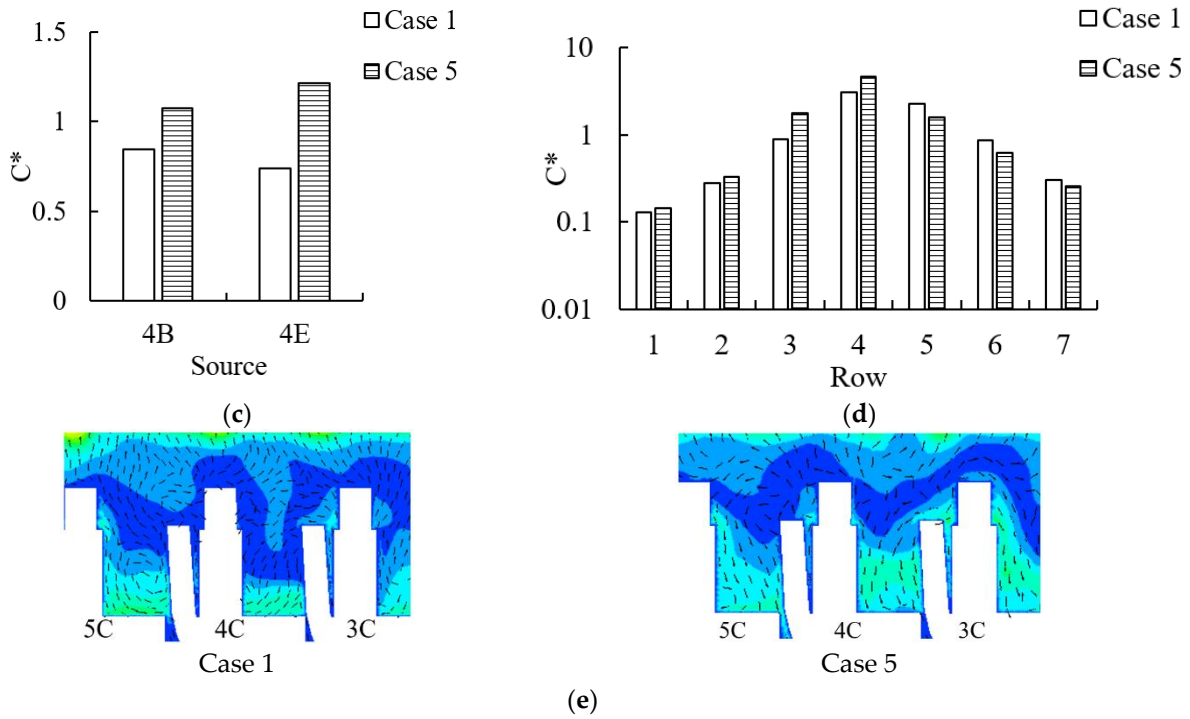

Figure 12. Airflow and normalized pollutant concentration distribution when misaligning the seat rows in Case 5: (**a**) air flow distribution in the cross-section across the heads of passengers in 4A to 4C, (**b**) airflow distribution in the cross-section across the heads of passengers in 4D to 4F, (**c**) comparison of the average pollutant concentration in respiratory zone of passengers in the half cabin opposite to the pollutant source between Cases 1 and 5, (**d**) comparison of the average pollutant concentrations in respiratory zone of the passengers in each row for the pollutant source at 4B, (**e**) airflow distribution in the longitudinal section from seats 3C to 5C in Cases 1 and 5.

Figure 12c shows the modeled average concentration in respiratory zones of the 21 passengers in the half cabin opposite to the pollutant release source in Cases 1 and 5, in which the pollutant sources at 4B and 4E were considered. When compared with the symmetric seat layout in Case 1, the seat misalignment increased the pollutant concentration in the respiratory zone of seats 4D to 4F for the pollutant source at 4B by 24%. The pollutant concentration increased by 64% for the pollutant source at 4E. This implied that the misalignment of seat rows had clearly weakened the block effect of the air curtain in the aisle.

Figure 12d presents the modeled average pollutant concentration in the respiratory zone of each row for the pollutant source of 4B. The pollutant concentrations in Case 5 were higher than those in Case 1 in rows 1 to 3 and lower than those in Case 1 in rows 5 to 7. This implied that the seat row misalignment did not much impact the basic distribution of the pollutant concentration in the longitudinal section. There was also a minimal difference in the airflow between Cases 1 and 5, as shown in Figure 12e.

4. Discussion

In this investigation, the validated CFD model was used to study the airflow and pollutant transport in five cases. This study adopted a simplified manikin geometry model to simulate a passenger. The body profiles of the manikins would affect the airflow pattern and the transport of pollutant in the vicinity of the body [34,35]. However, a high-resolution streamlined body geometry would demand tremendous computing resources. Most investigations [11,14,22,23] adopted simplified manikins for simplicity. In addition, previous investigation [36] found that there was no big difference in the macroscopic airflow patterns between a real-shaped manikin and a simplified manikin. Therefore, this study

used a rectangular block to represent a passenger. Furthermore, this investigation used the same manikin model for all of the passengers, which was apart from reality. The diversity of passenger geometry, such as the geometry of adults, children of different ages, and even adults with different weights, could be accounted for in future exploration. Note that the passengers in different body geometries could cause different heights in their breathing zones, for which the pollutant concentrations might vary greatly.

In addition, numerous combinations of seat inclination existed in reality, with an inclined seat at a random position. The remaining seat inclination situations could still be further investigated in the future. Moreover, during the flight multiple passengers are breathing at the same time in the cabin. The passengers with pollutant release may be in random seats. Due to the limitation of computing resources, this investigation considered only three typical situations of seat inclination and focused on the pollutant release from the exhalation of only one passenger.

In this study, the modeled pollutant concentrations in the half cabin opposite to the pollutant source were adopted to evaluate the cross-contamination. The changes in modeled pollutant concentrations in each row with different seat layouts were used to study the longitudinal transport of pollutants. The results implied that it is crucial to maintain the symmetric seat layout to minimize the cross-transport of pollutants. The asymmetric seat layout either by inclining random seats or misaligning the seat rows would strengthen the cross-contamination in an aircraft cabin.

5. Conclusions

This investigation used the validated CFD program to evaluate the impacts of seat inclination and misalignment of seat rows on the airflow and pollutant transport in a single-aisle aircraft cabin. The conclusions are as follows:

The inclination of only three adjacent seats in a whole cabin did not change the flow and the pollutant transport in the cross-section very much. However, the seat inclination resulted in an increase in the pollutant concentration in the respiratory zone of the rear three rows while the pollutant concentration in the respiratory zone of the front three rows decreased, if the pollutant was released from a passenger in an inclined seat.

The inclination of all of the seats in a half cabin while the other half cabin without seat inclination and the misalignment of seat rows resulted in a highly asymmetric seat layout. In such situations, the supplied air jets from both sides could easily penetrate the air curtain in the aisle and promote cross-contamination.

There was no meaningful difference in the flows and pollutant concentration distribution when maintaining the symmetric seat layout with either all of the upright seats or all of the inclined seats. A symmetric seat layout aids in circumscribing the released pollutants in a small region and reducing the contamination both in the cross and the longitudinal sections.

Based on the above findings, it is highly recommended to maintain all of the seats in an upright manner or be inclined completely on flights. Any random inclination of seats or misalignment of seat rows that results in a highly asymmetric seat layout should be avoided during the pandemic.

Author Contributions: Conceptualization, T.Z.; methodology, T.Z. and S.L.; software, M.F.; validation, M.F.; investigation, M.F.; writing—original draft preparation, M.F.; writing—review and editing, T.Z. and S.L.; visualization, M.F.; project administration, T.Z. All authors have read and agreed to the published version of the manuscript.

Funding: This study was partially supported by the National Natural Science Foundation of China (NSFC) through Grant No. 52108084.

Conflicts of Interest: The authors declare that they have no known competing financial interests or personal relationships that could have appeared to influence the work reported in this paper.

Appendix A

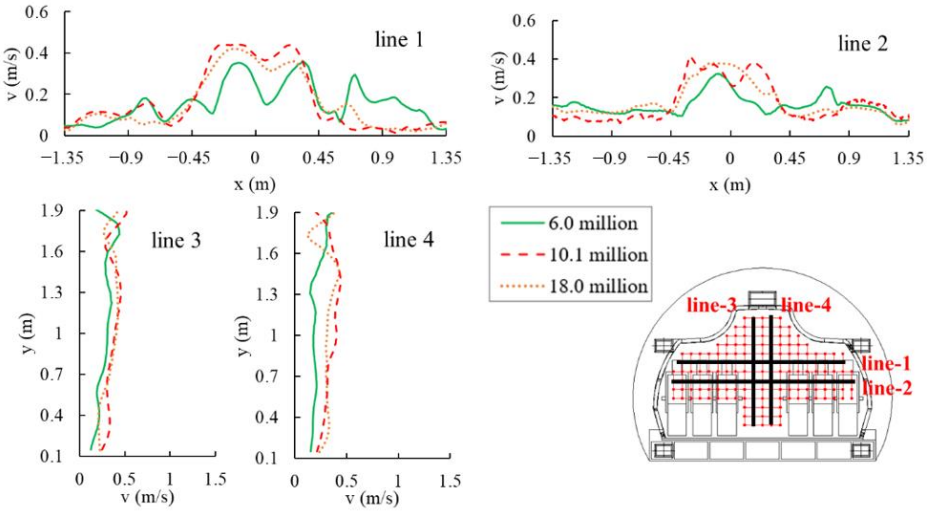

Figure A1. Grid independence test for air velocity in the cross-section.

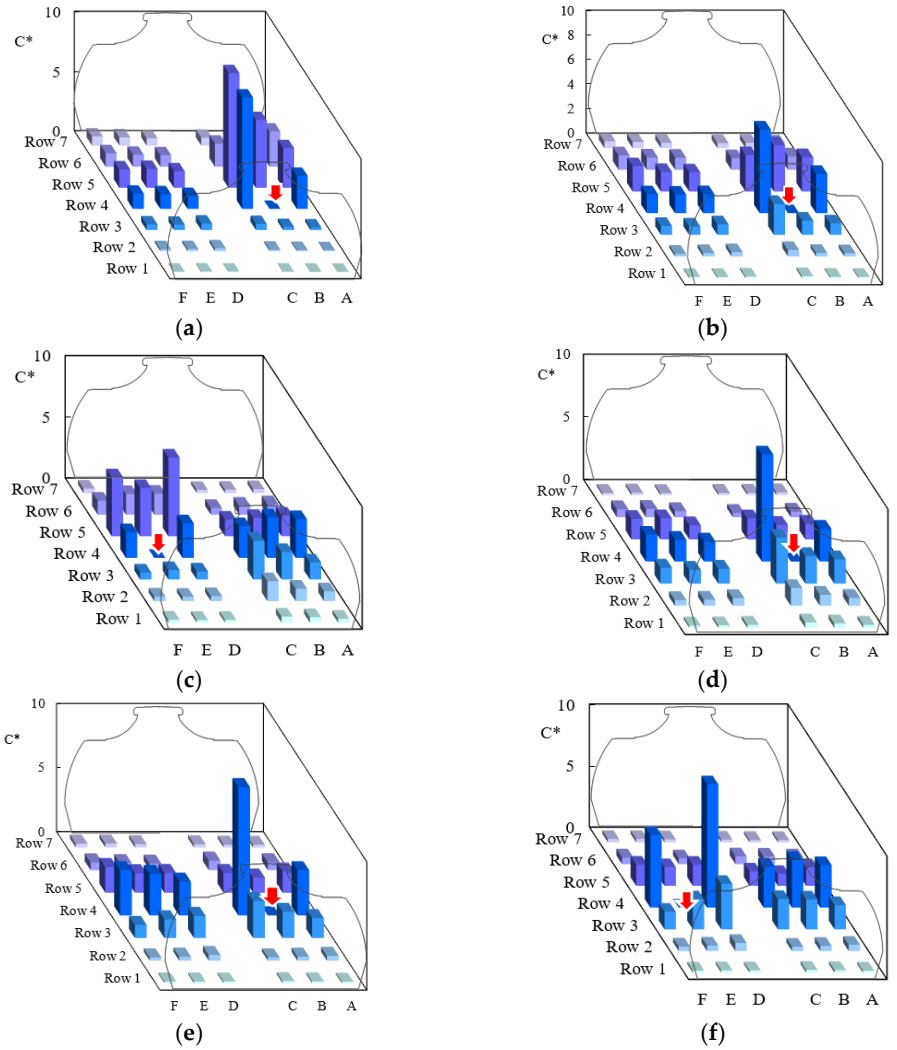

Figure A2. Normalized pollutant concentrations in the respiratory zone of passengers in different seats: (**a**) Case 2 (source: 4B), (**b**) Case 3 (source: 4B), (**c**) Case 3 (source: 4E), (**d**) Case 4 (source: 4B), (**e**) Case 5 (source: 4B), (**f**) Case 5 (source: 4E).

References

1. Sotomayor-Castillo, C.; Radford, K.; Li, C.; Nahidi, S.; Shaban, R.Z. Air travel in a COVID-19 world: Commercial airline passengers' health concerns and attitudes towards infection prevention and disease control measures. *Infect. Dis. Health* **2021**, *26*, 110–117. [CrossRef] [PubMed]
2. Khanh, N.C.; Thai, P.Q.; Quach, H.L.; Thi, N.A.H.; Dinh, P.C.; Duong, T.N.; Mai, L.T.Q.; Nghia, N.D.; Tu, T.A.; Quang, L.N.; et al. Transmission of SARS-CoV 2 During Long-Haul Flight. *Emerg. Infect. Dis.* **2020**, *26*, 2617–2624. [CrossRef] [PubMed]
3. WHO. Modes of Transmission of Virus Causing COVID-19. In *Implications for IPC Precaution Recommendations: Scientific Brief*; World Health Organization: Geneva, Switzerland, 2020.
4. Yan, Y.; Li, X.; Shang, Y.; Tu, J. Evaluation of airborne disease infection risks in an airliner cabin using the Lagrangian-based Wells-Riley approach. *Build. Environ.* **2017**, *121*, 79–92. [CrossRef] [PubMed]
5. Mangili, A.; Gendreau, M.A. Transmission of infectious diseases during commercial air travel. *Lancet* **2005**, *365*, 989–996. [CrossRef]
6. Hanna, S. Transport and dispersion of tracers simulating COVID-19 aerosols in passenger aircraft. *Indoor Air* **2021**, *32*, e12974. [CrossRef]
7. Zee, M.; Davis, A.C.; Clark, A.D.; Wu, T.; Jones, S.P.; Waite, L.L.; Cummins, J.J.; Olson, N.A. Computational Fluid Dynamics Modeling of Cough Transport in an Aircraft Cabin. *Sci. Rep.* **2021**, *11*, 23329. [CrossRef]
8. Hunt, E.H.; Reid, D.H.; Space, D.R.; Tilton, F.E. Commercial airliner environmental control system. In Proceedings of the Aerospace Medical Association Annual Meeting, Anaheim, CA, USA, 7–11 May 1995.
9. Zhang, T.; Li, P.; Zhao, Y.; Wang, S. Various air distribution modes on commercial airplanes, Part 1: Experimental measurement. *HVACR Res.* **2013**, *19*, 457–470.
10. Zhang, T.; Li, P.; Zhao, Y.; Wang, S. Various air distribution modes on commercial airplanes, Part 2: Computational fluid dynamics modeling and validation. *HVACR Res.* **2013**, *19*, 457–470.
11. Zhang, T.; Chen, Q. Novel air distribution systems for commercial aircraft cabins. *Build. Environ.* **2007**, *42*, 1675–1684. [CrossRef]
12. You, R.; Lin, C.-H.; Wei, D.; Chen, Q. Evaluating the commercial airliner cabin environment with different air distribution systems. *Indoor Air* **2019**, *29*, 840–853. [CrossRef]
13. Cao, Q.; Liu, M.; Li, X.; Lin, C.H.; Wei, D.; Ji, S.; Zhang, T.T.; Chen, Q. Influencing factors in the simulation of airflow and particle transportation in aircraft cabins by CFD. *Build. Environ.* **2022**, *207*, 108413. [CrossRef]
14. Wan, M.P.; Sze To, G.N.; Chao, C.Y.H.; Fang, L.; Melikov, A. Modeling the Fate of Expiratory Aerosols and the Associated Infection Risk in an Aircraft Cabin Environment. *Aerosol Sci. Technol.* **2009**, *43*, 322–343. [CrossRef]
15. Zhang, Z.; Chen, X.; Mazumdar, S.; Zhang, T.; Chen, Q. Experimental and numerical investigation of airflow and contaminant transport in an airliner cabin mockup. *Build. Environ.* **2009**, *44*, 85–94. [CrossRef]
16. Sagnik, M.; Chen, Q. Influence of cabin conditions on placement and response of contaminant detection sensors in a commercial aircraft. *J. Environ. Monit.* **2008**, *10*, 71–81.
17. Li, J.; Cao, X.; Liu, J.; Wang, C.; Zhang, Y. Global airflow field distribution in a cabin mock-up measured via large-scale 2D-PIV. *Build. Environ.* **2015**, *93*, 234–244. [CrossRef]
18. Li, J.; Liu, J.; Wang, C.; Wesseling, M.; Müller, D. PIV experimental study of the large-scale dynamic airflow structures in an aircraft cabin: Swing and oscillation. *Build. Environ.* **2017**, *125*, 180–191. [CrossRef]
19. Wang, C.; Liu, J.; Li, J.; Guo, Y.; Jiang, N. Turbulence characterization of instantaneous airflow in an aisle of an aircraft cabin mockup. *Build. Environ.* **2017**, *116*, 207–217. [CrossRef]
20. Li, X.; Zhang, T.; Fan, M.; Liu, M.; Chang, D.; Wei, Z.; Lin, C.-H.; Ji, S.; Liu, J.; Shen, S.; et al. Experimental evaluation of particle exposure at different seats in a single-aisle aircraft cabin. *Build. Environ.* **2021**, *202*, 108049. [CrossRef]
21. Liu, M.; Chang, D.; Liu, J.; Ji, S.; Lin, C.H.; Wei, D.; Long, Z.; Zhang, T.; Shen, X.; Cao, Q.; et al. Experimental investigation of air distribution in an airliner cabin mockup with displacement ventilation. *Build. Environ.* **2021**, *191*, 107577. [CrossRef]
22. Li, B.; Duan, R.; Li, J.; Huang, Y.; Yin, H.; Lin, C.H.; Wei, D.; Shen, X.; Liu, J.; Chen, Q. Experimental studies of thermal environment and contaminant transport in a commercial aircraft cabin with gaspers on. *Indoor Air* **2016**, *26*, 806–819. [CrossRef]
23. Khaled, T.; Mohamed, A.; Omar, A.M.; Anderoglu, O.; Poroseva, S.V. Simulation of aerosol transmission on a Boeing 737 airplane with intervention measures for COVID-19 mitigation. *Phys. Fluids* **2021**, *33*, 033312.
24. Li, F.; Liu, J.; Pei, J.; Chen, Q. Experimental study of gaseous and particulate contaminants distribution in an aircraft cabin. *Atmos. Environ.* **2014**, *85*, 223–233. [CrossRef] [PubMed]
25. Yan, Y.; Li, X.; Fang, X.; Tu, J. Transmission of COVID-19 virus by cough-induced particles in an airliner cabin section. *Eng. Appl. Comput. Fluid Mech.* **2021**, *15*, 934–950. [CrossRef]
26. Gupta, J.K.; Lin, C.-H.; Chen, Q. Transport of expiratory droplets in an aircraft cabin. *Indoor Air* **2010**, *21*, 3–11. [CrossRef]
27. Wang, W.; Wang, F.; Lai, D.; Chen, Q. Evaluation of SARS-COV-2 transmission and infection in airliner cabins. *Indoor Air* **2022**, *32*, e12979. [CrossRef]
28. ASHRAE. *2019 Ashrae Handbook Heating, Ventilating, and Air-Conditioning Application SI Edition. Ashrae Hvac Applications Ip Handbook-2019*; ASHRAE: Atlanta, GA, USA, 2019.
29. Gupta, J.K.; Lin, C.H.; Chen, Q. Characterizing exhaled airflow from breathing and talking. *Indoor Air* **2010**, *20*, 31–39. [CrossRef]
30. Liu, S.; Xu, L.; Chao, J.; Shen, C.; Liu, J.; Sun, H.; Xiao, X.; Nan, G. Thermal environment around passengers in an aircraft cabin. *HVACR Res.* **2013**, *19*, 627–634.

31. Fabian, P.; McDevitt, J.J.; DeHaan, W.H.; Fung, R.O.P.; Cowling, B.J.; Chan, K.H.; Leung, G.; Milton, D.K. Influenza virus in human exhaled breath: An observational study. *PLoS ONE* **2008**, *3*, e2691. [CrossRef]
32. Li, M.; Yan, Y.; Zhao, B.; Tu, J.; Liu, J.; Li, F.; Wang, C. Assessment of turbulence models and air supply opening models for CFD modelling of airflow and gaseous contaminant distributions in aircraft cabins. *Indoor Built Environ.* **2018**, *27*, 606–621. [CrossRef]
33. Schatzmann, M.; Olesen, H.; Franke, J. *COST 732 Model Evaluation Case Studies: Approach and Results*; Meteorological Institute: Hamburg, Germany, 2010.
34. Zukowska, D.; Melikov, A.; Popiolek, Z. Impact of geometry of a sedentary occupant simulator on the generated thermal plume: Experimental investigation. *HVACR Res.* **2012**, *18*, 795–811.
35. Melikov, A. Breathing thermal manikins for indoor environment assessment: Important characteristics and requirements. *Eur. J. Appl. Physiol.* **2004**, *92*, 710–713. [CrossRef] [PubMed]
36. Nielsen, P.V. Benchmark test for a computer simulated person. *Indoor Air* **2003**, *14*, 144–156.